Discovering Pareto-optimal magnetic-design solutions via a Generative Adversarial Networks (GAN)

Marco Baldan[1] and Paolo Di Barba[2]
[1]Fraunhofer Institute for Industrial Mathematics, ITWM, Kaiserslautern 67663 Germany
[2]Department of Electrical, Computer and Biomedical Engineering, University of Pavia, 27100 Pavia Italy

In the framework of induction hardening, the coil design task is particularly suitable to be formulated as multi-objective optimization problem. In fact, the Pareto front estimation raises the issue of guaranteeing a satisfactory diversity and number of non-dominated solutions to be provided to the decision maker (DM). In this paper, a generative adversarial network (GAN) and a forward neural network (FNN), which is cascade connected to the GAN generator, produce additional Pareto optimal solutions starting from the results of a genetic algorithm (NSGA-II) used as training set. The FNN ensures an accurate prediction of the objectives of the added solutions, removing the need for further field analyses. This method is first tested against a set of analytical problems and subsequently validated on a 3-objective coil design task to illustrate its utility for a real-world case.

Index Terms—**Design Optimization, GAN, Heat Treatment, Magnetic Field, Neural Networks, Pareto Optimization.**

I. Introduction

In induction hardening, the heat provided by the induced eddy currents and, if present, in a much minor intensity, by the hysteresis losses, is responsible for making the transformation in austenite happen. This is usually limited to the piece's boundary that is why the expression "induction hardening" often entails the concept of "induction surface hardening". During the subsequent quenching, the austenitic layer mostly transforms into martensite, which is characterized by an elevate hardness and has a slightly higher volume than the starting microstructure. The volume increase is responsible for surface residual compressive stresses. Benefits of induction hardening concern an augmented wear resistance of the piece, because of its direct correlation with hardness, and an increment of fatigue life due to a soft core and surface compressive stresses [1], [2]. If on one hand the regime parameters (power, heating time, frequency) affect the thickness of the hardening depth, on the other hand, the coil geometry shapes the hardened contour. Therefore, complex patterns to be hardened often requires non-trivial coil geometries. The coil design employs typically a software driven approach, in which an optimization algorithm (single or multi-objective, and usually evolutionary [3]) is coupled with the field analysis (frequently FEM) in order to estimate objectives and constraints.

Recently, machine learning has been increasingly adopted in business, life science and engineering. Electromagnetics has not been indifferent to this advance and, for instance, deep learning techniques begin to be used for field analyses too [4], [5]. Fully unsupervised approaches have been reported too [6], [7]. This paper will focus on a generative adversarial network (GAN) [8], a type of generative model capable of learning the regression distribution over data in an adversarial manner. They have been already successfully applied in many areas, like image generation and image super-resolution. Looking at electromagnetics, recent works show their use in magnetic resonance imaging [9] [10], antenna Q-factor characterization [11], scattering problems [12]. In this paper, a GAN is trained making use of the data derived from a multi-objective optimization problem solved with NSGA-II. Aiming, with the GAN generator, at discovering new Pareto optimal solutions in the design space, the GAN training set is composed of both Pareto optimal and non-optimal individuals. With reference to the discriminator, the former are labelled as real, the latter as fake. Moreover, a forward neural network (FNN) that takes the design variables as input and the objectives as output estimates, without the need of additional field analyses, the objective function values. Our approach significantly differs from [13], where a multi-objective evolutionary algorithm driven by GANs was proposed. Indeed, we separate the evolutionary search from the use of the GAN and we introduce a FNN. Moreover, the present work is not limited to analytical test problems but it is also based on the optimal design of a coil for induction hardening. In this sense, it is an innovative approach in the field of magnetism. The paper is organized as follows. Section II summarizes the proposed approach, while sections III and IV illustrate the analytical and real test cases.

Manuscript received February 07, 2022; revised August 26, 2015. Corresponding author: Paolo Di Barba (email: paolo.dibarba@unipv.it).

II. The Proposed Approach

A multi-objective optimization problem takes this form:

$$\min_{\mathbf{x}\in X} \mathbf{F}(\mathbf{x}) = (f_1(\mathbf{x}), ..., f_M(\mathbf{x})) \tag{1}$$

where X is the search space of design variables, $M > 1$ is the number of objectives, and $\mathbf{x} = (x_1, ..., x_N)$ is the design vector with N denoting the number of design variables [14]. The Pareto dominance relationship is here adopted to distinguish the qualities of two different solutions. The collection of all the Pareto optimal solutions in the design space defines the Pareto optimal set. Within this work, to solve (1) the well-known NSGA-II algorithm is adopted [15]. This defines the first step of the proposed approach, whose output is characterized by the collection of all individuals gathered in archives $\mathcal{A}_{\mathbf{x}} = X_{\mathbf{p}} \cup X_{\mathbf{d}}$ ($X_{\mathbf{p}}$ and $X_{\mathbf{d}}$ stand for the collection

of Pareto optimal and non-optimal solutions, respectively) and $\mathcal{A}_{\mathbf{F}} = F_{\mathbf{p}} \cup F_{\mathbf{d}}$, with $F_{\mathbf{p}} = \mathbf{F}(X_{\mathbf{p}})$ and $F_{\mathbf{d}} = \mathbf{F}(X_{\mathbf{d}})$, relevant to both design and objective spaces. We would like to underline that, in the proposed approach, no hypotheses regarding the shape of the Pareto front and the Pareto set are made.

The second step of our approach involves a GAN to discover (i.e. generate) new non-dominated solutions in the design space. A GAN consists of a generator (G) and a discriminator (D). Denoting by $\boldsymbol{\theta}_G$ the parameters of the generator and by $\mathbf{z}$ the input noise sampled from a latent variable that G receives (usually being the normal distribution $P_{\mathbf{z}}(\mathbf{z}) \approx \mathcal{N}(0, \sigma)$), the generated samples are indicated as $\hat{\mathbf{x}}$. In turn, the discriminator, whose parameters are indicated with $\boldsymbol{\theta}_D$, receives as input the Pareto optimal set ($P_{\mathbf{p}}$ indicates the distribution of $X_{\mathbf{p}}$) that is labelled as real, but also $P_{\mathbf{d}}$ (i.e. distribution associated to $X_{\mathbf{d}}$), classified as fake. D and G are trained playing the following two-player minimax game:

$$\arg\min_{\boldsymbol{\theta}_G} \max_{\boldsymbol{\theta}_D} V(D,G) = \mathbb{E}_{\mathbf{p}\sim P_{\mathbf{p}}}[\log(D(\mathbf{p}))] + \mathbb{E}_{\mathbf{d}\sim P_{\mathbf{d}}}[1 - \log(D(\mathbf{d}))] + \mathbb{E}_{\mathbf{z}\sim P_{\mathbf{z}}}[1 - \log(D(G(\mathbf{z})))] \quad (2)$$

where $D(\mathbf{p})$, $D(\mathbf{d})$, $D(G(\mathbf{z}))$ express the output of the discriminator with the real (Pareto optimal), fake (Pareto non-optimal), and generated sample, respectively. In Eq. 2, $\mathbb{E}_{\mathbf{h}\sim P_{\mathbf{h}}}$ denotes the expectation that vector $\mathbf{h}$ exhibits a distribution $P_{\mathbf{h}}$. Note that the second term at the right hand side does not appear in the original formulation [8] but we observed to be highly beneficial in our problem since it makes the discriminator, and as a consequence also the the generator, more robust (Fig. 1). We conjecture that the global optimum of Eq. 2 corresponds to $P_{G(\mathbf{z})} = P_{\mathbf{p}}$. The output of this second step concerns a collection of (ideally) non-dominated solutions in the design space obtained from the generator. How many they are is set by the DM. Only feasible individuals (i.e. fulfilling $\mathbf{x} \in X$ in Eq. 1) are further considered.

Finally, in the third step, a FNN (multilayer perceptron) is trained with $\mathcal{A}_{\mathbf{x}}$ and $\mathcal{A}_{\mathbf{F}}$ to approximate the forward problem solution ($\mathbf{x}$ as input, $\mathbf{F}$ as output) [16]. This allows to estimate in an inexpensive way the objectives of the feasible individuals generated in step two (Fig. 1).

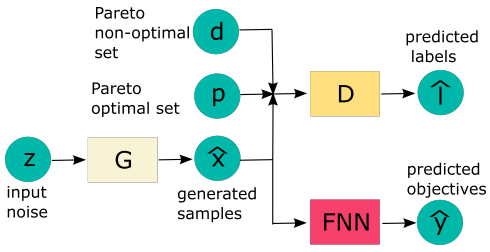

Fig. 1. General scheme of the GAN-based proposed approach.

III. Analytical Test Case

We will describe only two test cases, out of the several ones that we considered, the first based on the Fonseca-Fleming function with $N = 10$ and $X = [-4, 4]^N$. The solution is characterized by a non-convex Pareto front (see Fig. 2).

To solve the multi-objective problem, NSGA-II was run with a population of 100 individuals for 100 generations. Both GAN generator and discriminator have two hidden layers, the former with 24, the latter with 64 neurons each. LeakyReLU activation was used, except at the output layer of D, where sigmoid was preferred. The generator input noise has dimension 5. FNN has instead three hidden layers with 96 neurons each. This choice is the result of a trial and error approach. The number of epochs was set to 10^2. Computation was performed on TensorFlow. Fig. 2 shows the 53 Pareto optimal solutions obtained from NSGA-II and the 500 (also a different number could be set) solutions generated by GAN. Among 500, in this case all feasible, only 15 solutions result (in a Paretian sense) to be dominated by the solutions of NSGA-II. By the way, all dominated discovered solutions are located near the front.

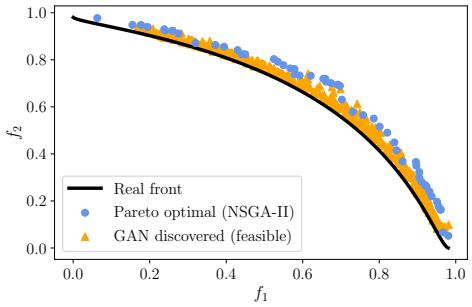

Fig. 2. GAN is able to learn the distribution of the Pareto optimal solutions.

So far, the analysis has been focused on the design space. However, it would be of relevance to know the values of the objectives (referring to the feasible discovered solutions) in an inexpensive way. And this especially in real cases where it could be expensive to evaluate the objectives. Therefore, the FNN (three hidden layers, each with 96 neurons, $\max(0, x^3)$ is the activation, 3 10^4 epochs) comes to our aid and gives an accurate but cheap estimate of them. The parity plot (not shown for brevity) highlights that the FNN is accurate in predicting the value of the objectives.

The second test case is based on the Kursawe function with $N = 3$ and $X = [-5, 5]^N$. The solution is characterized by disconnected regions in both Pareto front and Pareto set, making this test highly challenging. NSGA-II is run with a population of 60 individuals for 150 generations, thus obtaining 52 non-dominated solutions. Architectures of all neural networks are same as above. From the 500 solutions generated by the GAN, 430 result to be non-dominated by the NSGA-II Pareto front. Almost all discovered solutions ($\approx 95\%$) are clustered in the disconnected regions, showing this method is also applicable to disconnected Pareto sets (Fig. 3). The FNN performs well too.

IV. Real Test Case

Fig. 4 summarizes the system under study in which the longitudinal section of a cam that is supposed to be hardened in both nose and heel (i.e. along l_1 and l_2) is shown. The shape and position of a two-turn inductor is investigated to fulfil this

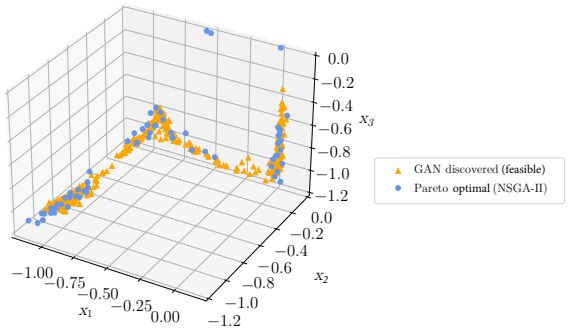

Fig. 3. GAN discovered solutions are clustered in the disconnected regions of the Pareto set (only $\approx 5\%$ are located in the regions in between).

task. Each turn is surrounded by flux concentrating material to enhance the induced power density. This is a common practise in induction hardening.

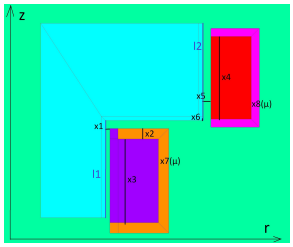

Fig. 4. Design variables of the system.

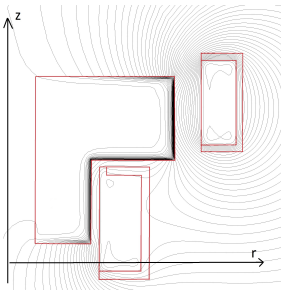

Fig. 5. Map of magnetic vector potential (amplitude, azimuthal component): cam, two-turn coil with flux guiding material.

We are aware that in designing an inductor for hardening applications, in order to describe the forward problem, multi-physical numerical simulations could be adopted [1]. For instance, they include the electromagnetic, thermal and metallurgical analyses. However, we will rely only on a non-linear time-harmonic FEM simulation. The reason is twofold. On the one hand, in real cases, heating time is often in the range of milliseconds. Therefore, in the first instance, the power induced distribution approximates the temperature and microstructural field relatively well. On the other, the principle purpose of this paper is to introduce an approach to augment the number of non-dominated design solutions. This is valid regardless of the simulation complexity. In total, 8 design variables have been selected (Fig. 4): 6 variables $(x_1, ..., x_6)$ define the shape and position of the turns, while x_7, x_8

TABLE I
DESIGN VARIABLES AND THEIR RANGES

Design variable	l_b	u_b
x_1 [mm]	0.5	2.0
x_2 [mm]	0.5	2.0
x_3 [mm]	4.0	15.0
x_4 [mm]	4.0	15.0
x_5 [mm]	1.0	4.0
x_6 [mm]	-3.0	3.0
x_7 [-]	1.0	40.0
x_8 [-]	1.0	40.0

l_b and u_b stand for the lower and upper bounds, respectively.

specify the relative magnetic permeability of the concentrating material to be used around the turns. This allows to better balance the induced power along l_1 and l_2. Tab. I summarizes the allowed ranges of the design variables. Regarding the regime, frequency and inductor current are assumed constant and equal to 12 kHz and 1650 A, respectively. These values come from previous experiments with a similar set-up. The mesh is composed of approximately 19 10^3 elements and 14 10^3 nodes. With a penetration depth of roughly 0.2 mm, it is mandatory a higher element density near the surface (Fig. 6).

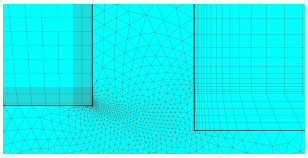

Fig. 6. Particular of the mesh: cam nose left side, upper turn right side.

The three following objective functions describe the quality, in terms of homogeneity and intensity, of the induced power distribution:

$$f_1(\mathbf{x}) = |P_{max}(\mathbf{x}, z, \mathbf{H}(\mathbf{x})) - P_{min}(\mathbf{x}, z, \mathbf{H}(\mathbf{x}))|, z \in l_1, l_2 \quad (3)$$

$$f_2(\mathbf{x}) = \int_{l_1,l_2} |P(\mathbf{x}, z, \mathbf{H}(\mathbf{x})) - P_{avg}(\mathbf{x}, \mathbf{H}(\mathbf{x}))| dz \quad (4)$$

$$f_3(\mathbf{x}) = -\int_{l_1,l_2} P(\mathbf{x}, z, \mathbf{H}(\mathbf{x})) dz \quad (5)$$

Eqs. 3, 4, 5 are to be simultaneously minimized with respect to $\mathbf{x}$. Like in the analytical case study, NSGA-II is adopted to collect a significant amount of non-dominated solutions. With a population of 56 individuals, after 150 generations, 81 non-dominated individuals were obtained. As in the previous section, a GAN and a FNN are trained making use of all (i.e. dominated and not) individuals. Architectures and number of epochs are same as before. The DM would like to discover 50 new solutions. Among them, 14 are non-feasible, 6 result dominated (in Paretian sense) and 30 turn to be non-dominated (Fig. 7). Using parallel coordinates in Fig. 7 highlight that f_1 and f_2 show little conflict, contrary to f_1 and f_3 or f_2 and f_3. Fig. 8 depicts several inductor geometries of 3 different non-dominated designs.

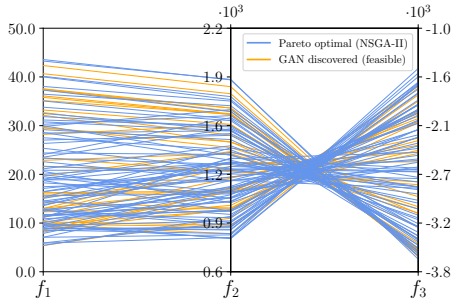

Fig. 7. Non-dominated (NSGA-II) and feasible GAN discovered solutions.

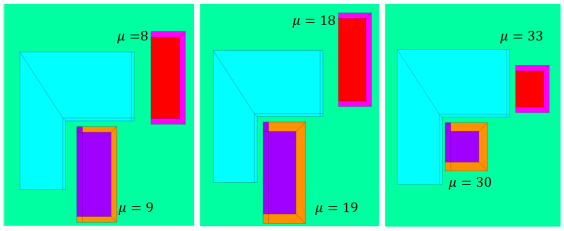

Fig. 8. Geometries of 3 different non-dominated solutions ($\min f_1, f_2, f_3$).

To test the effectiveness of the proposed method, the feasible proposed designs were evaluated with the FEM simulation in order to calculate the objectives. Fig. 9 compares FNN predictions with the FEM references, displaying an adequate agreement.

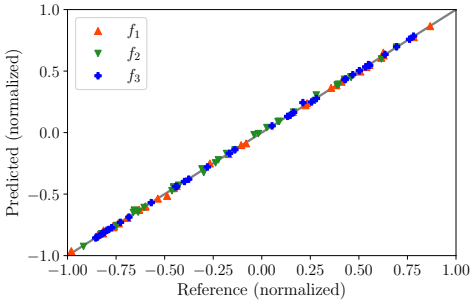

Fig. 9. Comparison between FEM simulated and FNN predicted (normalized) objectives in case of generated feasible designs by the GAN.

In this real test case, the non-negligible amount of non-feasible discovered solutions does not represent a critical aspect of the proposed approach. In fact, the DM could ask for more generated solutions in order to achieve an adequate density of the Pareto front. Considering, for instance, 1000 generated solutions, although 390 are non-feasible, 539 result actually to be non-dominated. Moreover, they are distributed on the entire front (Fig. 10). It follows that the front is now 7 times more dense. And this is not an upper limit, since the DM could ask for more solutions to be generated.

V. Conclusion

The proposed approach is able to discover new Pareto optimal solutions and to estimate their objective values without running new field simulations. This has been validated with analytical and real test cases. In both, compared to the results from NSGA-II, the front gets more dense of several times. All this occurs only at the cost of training a GAN and a FNN. Therefore, its application is particularly suitable to multi-objective problems involving expensive FEM analyses.

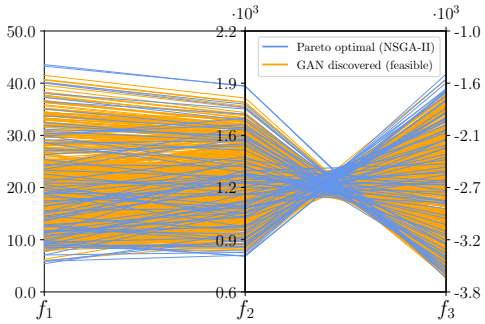

Fig. 10. Getting a more dense front due to discovered feasible solutions.

References

[1] M. Spezzapria, M. Forzan and F. Dughiero, "Numerical simulation of solid-solid phase transformations during induction hardening process," in *IEEE Transactions on Magnetics* vol. 52(3), 2016.
[2] D. Hmberg, Q. Liu, J. Montalvo-Urquizo, D. Nadolski, T. Petzold, A. Schmidt and A. Schulz, "Simulation of multi-frequency-induction-hardening including phase transformations and mechanical effects," in *Finite Elements in Analysis and Design* vol. 121, 2016, pp. 86-100.
[3] P. Di Barba, F- Dughiero, M. Forzan and E. Sieni, "Self-adaptive NGSA algorithm and optimal design of inductors for magneto-fluid hyperthermia," in *COMPEL* vol. 36(2), 2017, pp. 535-545.
[4] A. Khan, V. Ghorbanian and D. Lowther "Deep Learning for Magnetic Field Estimation," in *IEEE Trans. on Magnetics,* vol. 55(6), 2019.
[5] R. Gong and Z. Tang "Training Sample Selection Strategy Applied to CNN in Magneto-Thermal Coupled Analysis," in *IEEE Transactions on Magnetics,* vol. 57(6), 2021.
[6] P. Zhang, Y. Hu, Y. Jin, S. Deng, X. Wu and J. Chen "A Maxwell's Equations Based Deep Learning Method for Time Domain Electromagnetic Simulations," in *2020 IEEE Texas Symposium on Wireless and Microwave Circuits and Systems (WMCS)*, 2020.
[7] M. Baldan, G. Baldan and B. Nacke "Solving 1D non-linear magneto quasi-static Maxwell's equations using neural networks," in *IET Science, Measurement and Technology* vol. 15(2), 2021, pp. 204-217.
[8] I.J. Goodfellow, J. Pouget-Abadie, M. Mirza, B. Xu, D. Warde-Farley, S. Ozair, A. Courville and Y. Bengio "Generative adversarial networks," in *Advances in Neural Information Processing Systems*, 2014.
[9] M. Tian and K. Song "Boosting Magnetic Resonance Image Denoising With GANs," in *IEEE Access,* vol. 9, 2021, pp. 62266-62275.
[10] M. Jiang, Z. Yuan, X. Yang, J. Zhang, Y. Gong, L. Xia and T. Li "Accelerating CS-MRI Reconstruction With Fine-Tuning Wasserstein Generative Adversarial Network," in *IEEE Access,* vol. 7, 2019, pp. 152347-152357.
[11] J. Vijayamohanan, O. Noakoasteen, A. Gupta, M. Martinez-Ramon and C. G. Christodoulou "On Antenna Q-factor Characterization with Generative Adversarial Networks," in *IEEE Int. Symp. on Antennas and Propagation,* Montreal, Canada, 2020, pp. 1643-1644.
[12] Z. Ma, K. Xu, R. Song, C. Wang and X.Cheng "Learning-Based Fast Electromagnetic Scattering Solver Through Generative Adversarial Network," in *IEEE Trans. Antennas P.,* vol. 69(4), 2021, pp. 2194-2207.
[13] C. He, S. Huang, R. Cheng, K. Tan and Y. Jin "Evolutionary Multiobjective Optimization Driven by Generative Adversarial Networks (GANs)," in *IEEE Trans. on Cybernetics,* vol. 51(6), 2020, pp. 3129-3142.
[14] P. Di Barba, *Multiobjective Shape Design in El. and M.,* Springer, 2010.
[15] K. Deb, A. Pratap, S. Agarwal and T. Meyarivan "A fast and elitist multiobjective genetic algorithm: NSGA-II," in *IEEE Transactions on Evolutionary Computation,* vol. 6(2), 2002, pp. 182-197.
[16] M. Baldan, P. Di Barba and B. Nacke "Magnetic Properties Identification by Using a Bi-Objective Optimal Multi-Fidelity Neural Network," in *IEEE Trans. on Magnetics,* vol. 57(6), 2021.